Microfluidic In-Situ Spectrophotometric Approaches to Tackle Actinides Analysis in Multiple Oxidation States

Elodie Mattio, Audrey Caleyron, Manuel Miguirditchian, Amanda Lines, Samuel Bryan, Hope Lackey, Isaac Rodríguez-Ruiz, Fabrice Lamadie

Microfluidic in-situ spectrophometric approaches to tackle actinides analysis in multiple oxidation states

Journal:	*Applied Spectroscopy*
Manuscript ID	ASP-21-0254
Manuscript Type:	Submitted Manuscript
Date Submitted by the Author:	26-Aug-2021
Complete List of Authors:	Mattio, Elodie; CEA Caleyron, Audrey; CEA Miguirditchian, Manuel; CEA Bryan, Samuel A.; Pacific Northwest National Laboratory, Radiochemical Science and Engineering Lines, Amanda; Pacific Northwest National Laboratory, Radiochemical Science and Engineering Lackey, Hope E.; Pacific Northwest National Laboratory, Radiochemical Science and Engineering Rodriguez-Ruiz, Isaac; LGC Lamadie, Fabrice; CEA
Manuscript Keywords:	UV-vis Spectroscopy, Raman Spectroscopy, Opto/microfluidic, Photonic Lab-on-a-Chip, Uranium, Plutonium
Abstract:	The study and development of present and future processes for the treatment/recycling of spent nuclear fuels require many steps, from design in the laboratory to setting up on an industrial scale. In all of these steps, analysis and in-strumentation are key points. For scientific reasons (small-scale studies, control of phenomena, etc.) but also with regards to minimizing costs, risks, and waste, such developments are increasingly carried out on milli/microfluidic devices. The logic is the same for the chemical analyses associated with their follow-up and interpretation. Due to this, over the last few years opto/microfluidic analysis devices adapted to the monitoring of different processes (disso-lution, liquid/liquid extraction, precipitation, etc.) have been increasingly designed and developed. In this work we prove that photonic lab-on-a-chip (PhLoC) technology is fully suitable for all actinides concentration monitoring along the plutonium uranium refining extraction (PUREX) process. Several PhLoC microfluidic platforms were specifi-cally designed and used in different nuclear R&D laboratories, to tackle actinides analysis in multiple oxidation states even in mixtures. The detection limits reached (a few µmol.L^{-1}) are fully compliant with on-line process monitoring whereas a range of analyzable concentrations of three orders of magnitude can be covered with less than 150 µL of analyte. Finally, this work confirms the possibility and the potential of coupling Raman and UV-Visible spectrosco-pies at the microfluidic scale, opening the perspective of measuring very complex mixtures.

Microfluidic in-situ spectrophometric approaches to tackle actinides analysis in multiple oxidation states

Elodie Mattio[1], Audrey Caleyron[1], Manuel Miguirditchian[1], Amanda M. Lines[3], Samuel A. Bryan[3], Hope E. Lackey[3], Isaac Rodriguez-Ruiz[2], Fabrice Lamadie[1*]

[1] CEA, DES, ISEC, DMRC, Univ Montpellier, 30207 Bagnols-sur-Ceze, Marcoule, France

[2] Laboratoire de Génie Chimique - CNRS, UMR 5503, Toulouse, France.

[3] Pacific Northwest National Laboratory, Richland, Washington 99352, United States.

[*]Corresponding author: fabrice.lamadie@cea.fr

Abstract

The study and development of present and future processes for the treatment/recycling of spent nuclear fuels require many steps, from design in the laboratory to setting up on an industrial scale. In all of these steps, analysis and instrumentation are key points. For scientific reasons (small-scale studies, control of phenomena, etc.) but also with regards to minimizing costs, risks, and waste, such developments are increasingly carried out on milli/microfluidic devices. The logic is the same for the chemical analyses associated with their follow-up and interpretation. Due to this, over the last few years opto/microfluidic analysis devices adapted to the monitoring of different processes (dissolution, liquid/liquid extraction, precipitation, etc.) have been increasingly designed and developed. In this work we prove that photonic lab-on-a-chip (PhLoC) technology is fully suitable for all actinides concentration monitoring along the plutonium uranium refining extraction (PUREX) process. Several PhLoC microfluidic platforms were specifically designed and used in different nuclear R&D laboratories, to tackle actinides analysis in multiple oxidation states even in mixtures. The detection limits reached (a few µmol.L^{-1}) are fully compliant with on-line process monitoring whereas a range of analyzable concentrations of three orders of magnitude can be covered with less than 150 µL of analyte. Finally, this work confirms the possibility and the potential of coupling Raman and UV-Visible spectroscopies at the microfluidic scale, opening the perspective of measuring very complex mixtures.

Keywords

Uranium, Plutonium, UV-vis Spectroscopy, Raman Spectroscopy, Opto/microfluidic, Photonic Lab-on-a-Chip

INTRODUCTION

The development and study of new recycling processes for spent nuclear fuel rely, at all steps, on analysis and instrumentation. Moreover, for scientific reasons (small-scale studies, thermodynamic studies, etc.) but also to minimize costs, risks and waste, these developments are increasingly carried out on milli/microfluidic devices[1]. It is therefore mandatory to perform the associated chemical analyses at the same scale by implementing the techniques on microfluidic devices. Concretely, a microfluidic system allows handling fluids within channels whose dimensions are in the micrometer scale (from a few tens to a few hundreds), avoiding the effect of convective forces in solutions, and inducing a laminar flow. These devices permit the reduction of analyte consumption up to several orders of magnitude, well controlled fluid manipulation, lower cost and shorter analysis time than conventional systems. This is especially relevant when considering actinide analysis, which remains an important issue for R&D studies in this field.

There are many analytical methods for quantifying actinides in solution, from ICP-MS [2] to Raman [3] and UV-Visible spectroscopy [4], but few of them allow live, online monitoring of the small volumes, beneficial to the study of complex chemical and radioactive conditions encountered in actinide research. Among these methods, Raman spectroscopy and UV−vis absorbance are the most relevant analytical techniques to measure actinide concentrations in aqueous solutions. Absorption spectroscopy is widely used for the analysis of actinides in the nuclear industry, especially for uranium [4–6] and plutonium [7–9], which are the main elements involved in the PUREX (Plutonium, Uranium, Reduction, Extraction) process. These two actinides have the advantage of having f-f electronic transitions, which give characteristic absorption bands in the visible and near infrared, allowing direct quantification without prior treatment. This analytical method has also the advantage of being easily deployable and adaptable to more complex environmental conditions [10,11]. However, the use of absorbance for quantitative analysis of multicomponent solutions is less straightforward due to the possible existence of matrix effects, which can complicate an accurate determination [7]. Indeed, the quantification of actinides in HNO_3 acidic solutions is a clear example of the interference of matrix effects, which can be overcome by the combination of complementary analytical techniques [11]. Considering that Raman spectroscopy is sensitive to nitric acid concentration, the simultaneous coupling of both UV-visible and Raman spectroscopies provides a more complete analytical tool to monitor the PUREX process.

In the nuclear field, the use of microfluidic devices implementing analytical detection schemes addresses several major challenges: by reducing the volume of the sample and automating the measurement, microfluidic systems makes it possible to reduce the operator's exposure to ionizing radiation, but also reduces the exposure of the equipment used, which will be subjected to lower radiation doses, thus increasing its longevity. In addition, for use in a glove box, this technology reduces radioactive waste generation, both effluents and contaminated materials, and the size of the components in general is greatly reduced. In addition, when considering spectrometric detection schemes, all electronics can be remotely located outside the glove box (light sources, spectrometers, and computer).

A diverse range of materials to match chemical and irradiation resistance can be used for the microfluidic systems fabrication. In a previous study, we investigated the chemical and radiation resistance of these materials in more detail and compared their optical performance using microsystems fabricated in different materials, based on the analysis of lanthanides [12].

In this study, the evaluation of a complete optofluidic analytical approach, potentially combining both UV-Vis and Raman detection schemes, and suitable to be operated in a confined enclosure, such a glove box, will be carried out for the analysis of uranium (IV), uranium (VI), and plutonium (IV) pure solutions and mixtures, with the aim of subsequently developing microfluidic analytical systems resulting in the detection of actinides using both spectrophotometric techniques.

Analysis conditions of all the solutions have been defined according to the state of the art. Firstly, it is known that a significant variation in absorbance is observed as a function of the acid concentration. Several studies [7,13] show the strong influence of the concentration of nitric acid in the medium. For example, for Pu(IV), the increase in the acid concentration is accompanied by a decrease in the characteristic absorbance bands. In addition, a shift in the characteristic bands of Pu(IV) is also observed, particularly for the peak at 475 nm. This change in the maximum wavelength is due to Pu(IV) complexation by nitrate ions. Consequently, the nitric acid concentration will be clearly defined for each batch of samples. The measurements were carried out systematically from the maximum of absorbance and comparisons with the literature were made at similar concentrations. Secondly, the concentrations of HNO_3 for uranium solutions have been chosen to avoid the formation of colloids in solution [14] (these are formed at a pH between 1<pH<4).

Spectral overlap occurs for U(VI) and U(IV) in the UV-visible spectrum below 500 nm, which can complicate the quantification of U(VI) greatly when U(IV) is present even in very small amounts. However, previous demonstrations show the integration of Raman spectroscopy can provide additional insight into system chemistry and enable more accurate quantification of U(VI) in the presence of U(IV) [3]. In addition to U(VI) (uranyl) many PUREX relevant compounds are Raman active, including phosphate, nitrate, and water [3,15–19]. Raman spectroscopy can also provide insight into matrix conditions relevant to spent nuclear fuel reprocessing, such as pH; for instance, the Raman water vibrational band changes in response to acid concentration [20,21]. Raman spectroscopy can be used to detect UV-visible inactive molecules and polyatomic ions in aqueous and organic phase solutions, but it does not directly detect free, monoatomic ions. As such, Raman spectroscopy will detect U(VI) in the form of the dioxo-uranyl ion, but it will not detect U(IV) in the monoatomic cation form. The integration of Raman and UV-visible spectroscopy to monitor actinide and HNO_3 solutions on a single chip would allow for the quantification of acid concentration, U(VI), and U(IV) while avoiding overlapping spectral signals.

Following this introduction, this paper is structured in two parts. The first part introduces all the materials and methods used for the experiments. The second part highlights, on one hand, the results and limits of detection for pure analytes characterized by UV-Vis spectroscopy using a Photonic Lab on Chip (PhLoC) and, on the other hand, the possibility of processing binary mixtures of uranium oxidation states by means of a robust signal processing. In this part, the advantage of coupling UV-visible spectroscopy and Raman spectroscopy to improve results in specific configurations is also discussed. The conclusion summarizes the main results and proposes some perspectives.

MATERIALS AND METHODS

Solutions Preparation

U(IV) and U(VI) solutions: Nitric acid (ACS reagent, 70%) was purchased from Sigma-Aldrich. Stock uranium solutions at 216 $g.L^{-1}$ for U(VI) and at 308 $g.L^{-1}$ for U(IV) both in 1.35 M HNO3 were used as stock solutions. The U(IV) solution is supplemented with hydrazinium nitrate (at 0.1M) to maintain the uranium at the oxidation state IV in this nitric acid medium. From these two stock solutions, two sets were prepared by dilution using nitric acid of the same molar concentration. Analyte content was verified by inductively coupled plasma atomic emission spectrometry (ICP-AES). Subsequently, volumes were weighed using a precision scale and mother / daughter solutions densities were measured at 25 °C using a DMA 4500 density meter (Anton Paar, Germany) to calculate the final solution concentrations. Table 1 reports the concentrations achieved.

Pu(IV) solution: The plutonium solutions were prepared using a pure Pu(IV) solution with a concentration of 4.5 $g.L^{-1}$ in HNO_3 at 1.2 $mol.L^{-1}$. A calibration range between 0.05 and 4.5 $g.L^{-1}$ was prepared and the concentration was also checked by ICP-AES (Table 2). For further optical characterization, solution refractive indices were measured at 25 °C (at λ = 589 nm) using a RFM340 Abbe refractometer (Bellingham & Stanley).

PhLoC experimental setups

The PhLoC design relies on the concept of multiple path spectrophotometric configuration. It is described in great detail in [22,23] and can be made in different materials [12]. For uranium experiments, a PDMS (Sylgard 184 elastomer kit, supplied by Dow Corning, MI) chip was selected. For more details on the process of chip manufacturing by casting, the reader can refer to [23,24]. For plutonium, the analyses were performed in a glove box. Therefore, a glass chip (with an analogous design to the PDMS chip used for the uranium analyses), ensuring tighter and more robust fluidic connections, was mounted in a 3D-printed housing holding both fluidic and optical connections, and

subsequently inserted into the glove box. This chip was manufactured by FEMTOprint (Switzerland).

PhLoCs designs consist of a single microfluidic serpentine channel, with a total volume of ~3-5 µL, interrogated in 3 different regions describing optical paths (O.P.) of 1, 2.5, and 10 mm, respectively for the PDMS chip and 1.5, 3.5 and 15 mm for the glass-made chip. The interrogation regions are limited by 2D collimation microlenses, located on both sides and allowing an efficient coupling/decoupling of light to the system. Two air mirrors are placed along each side of the microfluidic channel to avoid light cross-contamination among channels. Self-aligning channels allow the hassle free positioning of pig-tailed 240 µm fiber optics (Thorlabs, Newton, NJ; NA = 0.22) into the micro optical setup. An overview of the PDMS chip filled with a 100 $g.L^{-1}$ U(IV) solution is shown on Fig. **1**a and a zoom on the three channels of the glass made chip is presented on Fig. **1**d.

For sample injection, two stainless steel needles (gauge 30, internal diameter 150 µm) were side-coupled and glued to the microfluidic channel, in order to provide a nearly zero-volume interface connection with any sample injector (external pumping systems, syringes, etc.), potentially allowing online sample feeding by means of standard Teflon or PEEK tubing. In all experiments, the chip was filled manually using directly connected syringes.

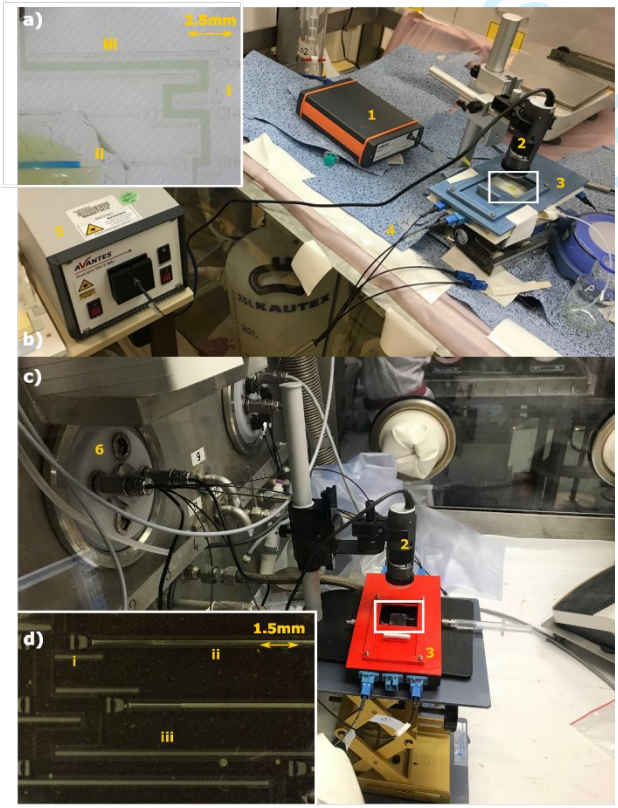

Fig. 1. a),d) Zoom of the PDMS chips for uranium (a) and glass chip for plutonium (d), using a handheld microscopic camera. The microlenses (i), self-aligning channels for fiber optics positioning (ii), and mirrors (iii), are visible. b), c) Setup implementation in a laboratory fume hood (b) and glove box (c): 1 - Spectrometer, 2 – Handheld microscopic camera, 3 – PhLoc inside its protection holder, 4 - Fibers optics, 5 - Balanced deuterium-halogen light source, 6 - Instrumented hole-plug.

Finally, for both assemblies, the chips were placed in a protective housing equipped with a lockable viewing hatch, which physically protects the chip and isolates it from the surrounding light sources.

An AvaLight-D(H)-S-BAL balanced deuterium-halogen light source and an Avaspec ULS2048CLEVO spectrometer (Avantes, Apeldoorn, The Netherlands) were used for light coupling and subsequent spectrum analysis. An overview of the setup is shown in Fig. **1**b and 1c.

The chip inside the glove box is connected to the light source and the spectrophotometer using fiber optics mounted on an instrumented hole-plug, which also connects the USB microscopic camera to the computer.

Particular attention was paid to the measurement protocol. Prior to each sample measurement, the microfluidic channel was air-dried by injecting air directly into the chip using a conventional syringe. The HNO_3 stock solution was used as a reference solution for absorbance calculation. A measurement of the reference intensity ("blank measurement", named I0) and of the background intensity ("dark measurement", named B) was performed every three sample intensity measurement (named I). A volume of 200 µL of each sample was used to ensure a complete, cleaning and correct filling of the microfluidic structure, and experiments were reproduced five times in order to assess the reproducibility of the methodology. For each measurement, the correct filling of the chip was checked with the microscopic camera, paying special attention to the absence of air bubbles within the optical interrogation regions.

Light intensity measurements were performed between 300 and 800 nm with a resolution of 0.56 nm fixed by the spectrometer in terms of pixel dispersion. Absorbance at $\lambda = 413.8$ nm for U(VI), $\lambda = 646.9$ nm for U(IV) and $\lambda = 477.7$ nm for Pu (IV) concentration respectively, have been calculated using the following expression:

$$A(\lambda) = \log_{10} \frac{I0(\lambda) - B(\lambda)}{I(\lambda) - B(\lambda)}$$

It is well known that when using the Beer-Lambert law, direct relationship between absorption and concentration remains valid only for low and intermediate concentrations. At high concentrations, deviations from linearity become important due to the increased effects of light scattering by the solution, especially refraction effects. In order to take this effect into account, the raw absorbance have been corrected according to the correction proposed in [25,26].

Raman Spectroscopy

Additional solutions containing uranyl nitrate (98.0-102%, Spectrum Chemical Manufacturing Corporation) and U(IV) with sodium nitrate (>99%, Sigma Aldrich) and nitric acid (70%, Sigma Aldrich) were made and measured on a fused silica microfluidic chip using Raman spectroscopy. The Raman setup has been described previously as have solution preparation approaches [3,18,27,28].

Table 1. Concentration ranges of U(IV) and U(VI) prepared for the experiments (uncertainties ± 2σ)

Targeted concentrations $g.L^{-1}$	0.10	0.20	0.50	1.00	2.00	5.00	10.00	20.00	30.00	40.00	50.00	100.00
U(IV) measured concentrations $g.L^{-1}$	0.11 ± 0.01	0.19 ± 0.01	0.49 ± 0.04	0.96 ± 0.03	1.99 ± 0.07	4.83 ± 0.10	9.75 ± 0.70	19.78 ± 0.60	28.98 ± 0.90	39.44 ± 0.90	46.12 ± 0.80	101.78 ± 0.95
U(VI) measured concentrations $g.L^{-1}$	0.10 ± 0.01	0.19 ± 0.01	0.49 ± 0.01	0.95 ± 0.04	2.02 ± 0.12	4.98 ± 0.12	10.79 ± 0.12	17.96 ± 0.46	27.76 ± 0.50	37.73 ± 1.00	46.95 ± 1.29	99.24 ± 1.54

Table 2. Concentration range of Pu(IV) prepared for the experiments (uncertainties ± 2σ)

Targeted concentrations $g.L^{-1}$	0.05	0.10	0.20	0.50	1.00	2.00	3.00	4.00	4.50
Pu(IV) measured concentrations $g.L^{-1}$	0.05 ± 0.01	0.11 ± 0.01	0.22 ± 0.01	0.56 ± 0.01	0.99± 0.02	2.18 ± 0.02	3.10 ± 0.01	3.87 ± 0.02	4.46 ± 0.07

RESULTS AND DISCUSSION

UV-Visible spectroscopy on Phlocs: Absorbance response, molar attenuation coefficient and detection limits for single actinide solutions

One of the main interests of Phlocs is that their monolithical integration of micro-optical elements and microfluidic channels in one single fabrication step makes them a low-cost analytical tool, easy to manufacture and implement. The counterpart of these advantages is that by design, they have a system of alignment and collimation of light less efficient than a traditional standard UV-Visible spectroscopy system. The fiber optics, which allow the light transmission from the source to the chip, and then from the chip to the spectrometer, are simply stripped and mechanically inserted into the guides and, as a consequence, they can be sensitive to several factors such as glove box depression, vibrations in the laboratory, adjacent activities, etc.

To evaluate the influence of these factors, we first performed a series of measurements on pure analytes in order to verify the stability and linearity of the response over process representative concentration ranges, the relevance of the molar attenuation coefficients and to determine the achievable detection limits according to the setups.

First, a light stability study was performed on all optical paths for both configurations by recording a spectrum every minute for 4 days. The results obtained show that the environmental factors induce a variation of less than 0.5% compared to the average signal over the 4 days. This variation was taken into account in the uncertainty calculation. In a second step, we have quantified for both uranium and plutonium the absorbance response as a function of the concentration. Figure 2 show the results obtained for U(IV), U(VI) and Pu(IV) respectively. In all cases, a linear relationship can be established between absorbance, and concentration and the R-Square coefficient confirms the quality of the fit. It can be noted that in the case of U(VI), the whole range can be measured on the channel of O.P.=10mm (the 3 orders of magnitude are fully covered). In the case of U(IV) and of Pu(IV), due to the high absorbance (e.g. almost four times higher for U(IV) than for U(VI) considering the same range) the use of two different optical paths (interrogation channels) becomes mandatory.

The quality of these results is confirmed when comparing the molar attenuation coefficients with the literature data as shown in Figure 3. For the three pure solutions, the molar attenuation coefficients calculated from the slope of the linear fit are in complete agreement with previous studies published in the state of the art, while the volumes of liquid involved are of the order of a few microliters (the internal volume of the chips varies between 3 and 5 µL).

Finally, the limits of detection were calculated in accordance to its IUPAC definition [29] as $LOD = k.sb/m$ (using a k value of 3, ensuring a confidence level of 99.86%), where the sensitivity, m, was obtained from the slopes of the least squares linear fitting for the previously mentioned plots and sb corresponds to the standard deviation of the blank (HNO_3 at 1.2 M and 1.35 M in our case) measured over 10 repetitions. LOD results are presented in Table 3.

Table 3. Limits of detection for pure analytes

	U(IV)	U(VI)	Pu(IV)
LOD (µmol.L^{-1})	26.2	88.2	10.2

These detection limits of a few tens of micro moles per liter, considering the ease of implementation and the low volume of effluent generated, confirms that Phlocs are definitely suitable to the on-line process monitoring.

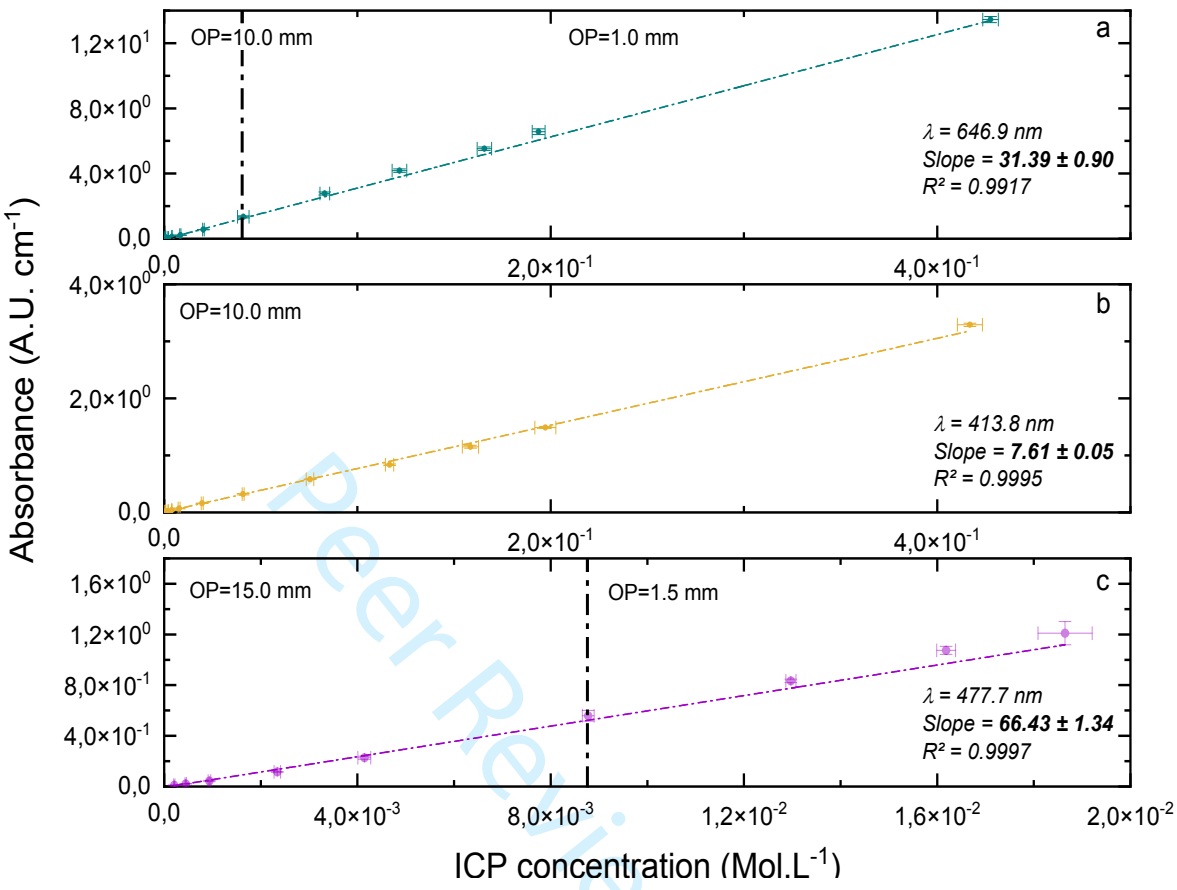

Fig. 2. a) Plot of the normalized absorbance measurements (in absorbance units (A.U.) cm^{-1}) as a function of U(IV) concentration. b) Plot of the normalized absorbance measurements (in absorbance units (A.U.) cm^{-1}) as a function of U(VI) concentration. c) Plot of the normalized absorbance measurements (in absorbance units (A.U.) cm^{-1}) as a function of Pu(IV) concentration. Lines represent the least-squares fitting of the experimental data.

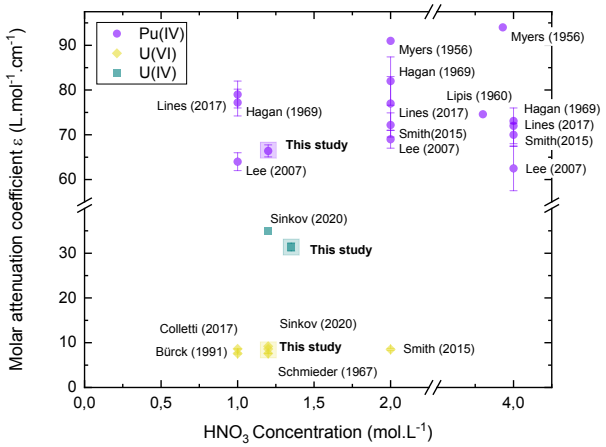

Fig. 3. Graphic comparison between the results obtained on optofluidic devices and the state of the art from the literature.

Uranium mixture measurements

The two previous responses of pure uranium solutions in both oxidation states were used for the analysis of uranium mixtures. To determine the proportion and the concentration of each oxidation state of uranium in a given mixture we considered that the absorbance at a given wavelength of the mixture is a linear combination of the absorbance of the pure solutions weighted by their respective proportions.

On this basis we can write that:

$$A_M(\lambda) = \alpha \times A_{U(IV)}(\lambda) + (1-\alpha) \times A_{U(VI)}(\lambda)$$

Where $A_M(\lambda)$ is the absorbance of the mixture at the wavelength λ, $A_{U(IV)}(\lambda)$ is U(IV) absorbance at the wavelength λ, $A_{U(VI)}(\lambda)$ is U(VI) absorbance at the wavelength λ and α the proportion of U(IV) in the mixture.

By exploiting this relationship at two wavelengths (here 413.6 and 649.6 nm), it is then possible to build a system of two equations with two unknowns that allows the simultaneous determination of the proportions and concentrations of each oxidation state.

First, the linearity of the response for mixtures was verified. For this purpose, two equivalent volumes (using a precision pipette) of U(VI) and U(IV) solutions at 10 $g.L^{-1}$ (≈ 42 $mM.L^{-1}$) were taken, mixed and the resulting mixture was measured on the chip. The absorbance response on the mixture was then compared to the response of pure solutions of U(VI) and U(IV) at 5 $g.L^{-1}$ (≈ 21 $mM.L^{-1}$). The results obtained are shown in on Fig. **4**. They clearly prove that the absorbance spectrum of the mixture can be found by linear composition of the absorbance

spectra of pure compounds. The same pure solutions at 10 g.L^{-1} were mixed by varying the proportions of U(VI) and U(IV) (10-90%, 25-75%, 50-50%, 75-25%, 90-10%) and in each case a linear response of the measurement system was observed and the total amount of uranium retrieved, as illustrated in the Table 4.

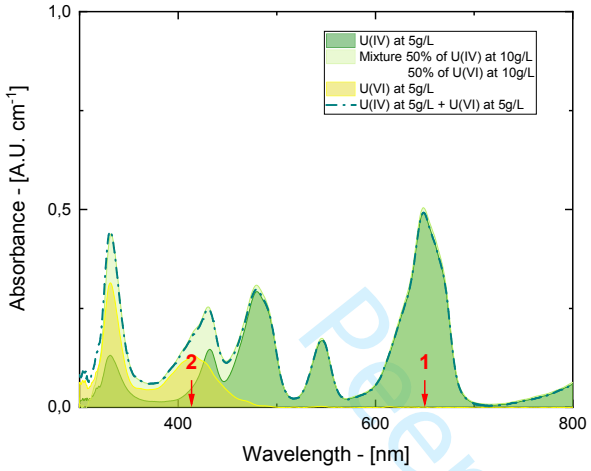

Fig. 4. Comparison between the absorbance spectrum of a 50/50 mixture of U(VI) and U(IV) at 10 g.L^{-1} and the absorbance spectra measured on pure U(VI) at 5 g.L^{-1} (yellow) and pure U(IV) at 5 g.L^{-1} (dark green). The dotted green line shows the sum of the absorbance spectra of the two pure compounds. The red arrows 1 and 2 denote the wavelengths used for the calculation of the mixtures.

Table 4 ICP-AES and UV-Visible spectroscopy measurements for five different mixtures of pure uranium solutions at 10 g.L^{-1}, ratio: 10% U(IV) / 90% U(VI) - 25% U(IV) / 75% U(VI) - 50% U(IV) / 50% U(VI) - 75% U(IV) / 25% U(VI) - 90% U(IV) / 10% U(VI).

	Mixture ratio	UV-Vis Spectroscopy (g.L^{-1})	ICP-AES (g.L^{-1})
U(IV)	10%	1.51±0.17	0.98±0.06
U(VI)	90%	8.85±0.12	8.75±0.28
U(IV)	25%	2.61±0.19	2.44±0.07
U(VI)	75%	6.36±0.10	7.29±0.20
U(IV)	50%	4.71±0.16	4.88±0.16
U(VI)	50%	4.43±0.27	4.86±0.07
U(IV)	75%	7.32±0.09	7.31±0.06
U(VI)	25%	2.46±0.03	2.43±0.03
U(IV)	90%	8.39±0.20	8.78±0.26
U(VI)	10%	0.97±0.06	0.97±0.03

Once linearity was confirmed, three tests on mixtures with increasing concentration of U(IV), of 0.5, 2.5 and 5 g.L^{-1}, were carried out. At each of these U(IV) concentrations, U(VI) concentration was the only variable parameter in this study (range of concentrations studied: 0.05, 0.1, 0.25, 0.5, 1.0 & 2.5 g.L^{-1}). This is totally justified because the analysis of the absorbance spectra clearly shows a near-zero absorbance of U(VI) in the U(IV) spectral measurement zone (noted 1 in Fig. **4**), whereas U(IV), on the other hand, has a non-negligible absorbance in the U(VI) measurement zone (noted 2 in Fig. **4**). Moreover, the absorbance of U(IV) is almost four times higher at equal concentration.

The concentrations and proportions of the two oxidation states of uranium were found by solving the system of equations below:

$$\begin{cases} A_M(\lambda_1) = \begin{pmatrix} \alpha \times \varepsilon_{U(IV)}(\lambda_1) \times C_{U(IV)} \\ +(1-\alpha) \times \varepsilon_{U(VI)}(\lambda_1) \times C_{U(VI)} \end{pmatrix} \times L \\ A_M(\lambda_2) = \begin{pmatrix} \alpha \times \varepsilon_{U(IV)}(\lambda_2) \times C_{U(IV)} \\ +(1-\alpha) \times \varepsilon_{U(VI)}(\lambda_2) \times C_{U(VI)} \end{pmatrix} \times L \end{cases}$$

Where L is the length of the optical path and ε is the molar attenuation coefficient at the considered wavelength for the considered oxidation state of uranium. In this case, $\lambda_1 = 649.9\ nm$ and $\lambda_2 = 413.6\ nm$.

Fig. **5** shows the results obtained with the three U(IV) concentrations considered. For all the experimental configurations, the respective concentrations of U(VI) and U(IV) are correctly determined. The adjustment of affine functions on the experimental points measured on U(VI) confirms that the experimental points are located as expected around the first bisector. This result is confirmed by the slopes of these adjustments as shown in the Table 5.

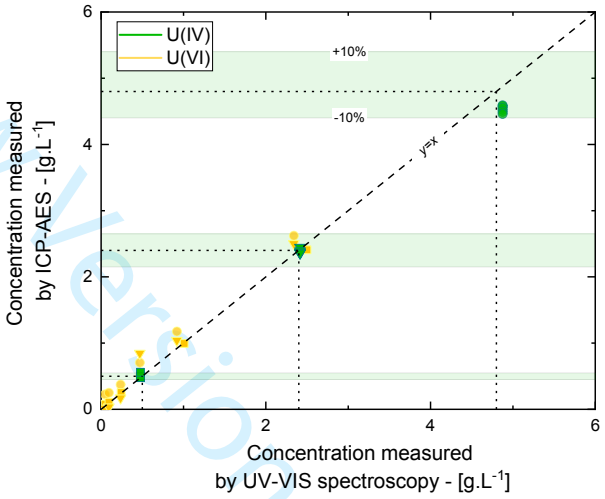

Fig. 5. Results obtained on U(IV)/U(VI) mixtures, the yellow symbols (triangles, squares, circles) show the results obtained on U(VI), the green symbols show the results obtained on U(IV) - The dotted lines indicate the values measured by ICP-AES. The error bars associated with the measurements have been intentionally excluded to make the figure easier to interpret.

Table 5. Linear fits of experimental points measured on U(VI) for the three mass concentrations of U(IV) considered.

U(IV) concentration (g.L^{-1})	Slope	Offset	R-Square
0.478	0.952 ± 0.001	0.031± 0.009	0.99973

2.415	1.079 ± 0.009	0.029± 0.095	0.97254
4.875	1.056 ± 0.019	0.169± 0.02	0.99867

The residuals analysis confirms these results. It shows that, logically, the greater the amount of U(IV), the more degraded the results of the U(VI) measurement become. Similarly, the impact of the absorbance of U(IV) in the U(VI) measurement zone is more significant for low mass concentrations of U(VI). Overall, he relative error for measurement in U(VI) remains acceptable above 0.2 $g.L^{-1}$ (≈850 $\mu mol.L^{-1}$), confirming again that this type of optofluidic device is well suited for R&D studies in process engineering.

The UV-visible absorbance spectral overlap of U(VI) and U(IV) can be addressed by the use of a secondary spectroscopic method in which limited interference occurs. U(VI) in the form of uranyl is Raman active while U(IV) in the form of the tetravalent cation is not. By simultaneously monitoring the U(IV) and U(VI) solutions using both UV-visible and Raman spectroscopy, enhanced insight into chemical composition can be gained.

Figure 6 shows the Raman response of aqueous solutions containing either U(VI) alone or both U(VI) and U(IV) in aqueous solutions of sodium nitrate and nitric acid. Preprocessing of baseline specified points using a 2nd order polynomial and normalization to the water band was used to reduce noise and make analyte bands more visible. As seen in Figure 6b, the presence of U(IV) in solution does not produce an interfering band in the Raman spectra, as shown in Figure 6a.

A response curve of these spectra is shown in Figure 6b. The total U(VI) range measured using Raman was 0.291 to 453 $g.L^{-1}$ U(VI). For the analysis here, data was limited to samples containing a maximum of 118 $g.L^{-1}$ U(VI) to better compare with the 100 $g.L^{-1}$ U(VI) maximum seen in other data sets. Points shown in green in Figure 6 indicate solutions that contain U(IV) and U(VI) together in solution, and these samples lie on the same response curve as solutions that contain U(VI) alone.

U(VI) was measured by Raman even in solutions containing a U(IV) : U(VI) ratio of 91:9%. Raman spectroscopy can clearly measure a large range of U(VI) concentrations, and due to the U^{4+} ion lacking a Raman fingerprint, mixtures of U(IV) and U(VI) can easily be measured. Spectral preprocessing was used to compensate for broad, complex baseline fluctuations caused by channel flexing during sample loading. An 11-points, square Savitsky-Golay smoothing filter was applied to produce the 2nd derivative of the original Raman spectra. After preprocessing, the Raman detection limit (calculated as in the IUPAC definition, above, using the standard deviation from 7 blanks) was determined to be 888 $\mu mol.L^{-1}$ U(VI) or 0.211 $g.L^{-1}$ U(VI). This is below the U(VI) concentrations measured by UV-visible spectroscopy in mixed U(VI)/U(VI) samples. It should also be noted that Raman detection limits can be improved by increasing the integration time. Data sets presented here were collected using a 3 second integration time; however this could be increased in future efforts in order to obtain a higher signal from the small sampling volume. Typically, a low integration time is preferable for online monitoring on microfluidic devices, where samples can pass the probe's focal point rapidly. Increasing the number of averaged spectra for each sample also improves detection limits; again, in rapidly changing systems, such averaging is not always possible.

While the Raman parameters used here resulted in a detection limit higher than that observed for the UV-vis, Raman spectroscopy provides a valuable tool for common working ranges in U materials processing. Additionally, Raman spectroscopy provides information of polyatomic analytes that are non-absorbing in the UV-visible range covered by many spectrometers, including nitrate ion and nitric acid, the concentrations of which are important parameters for spent fuel recycling.

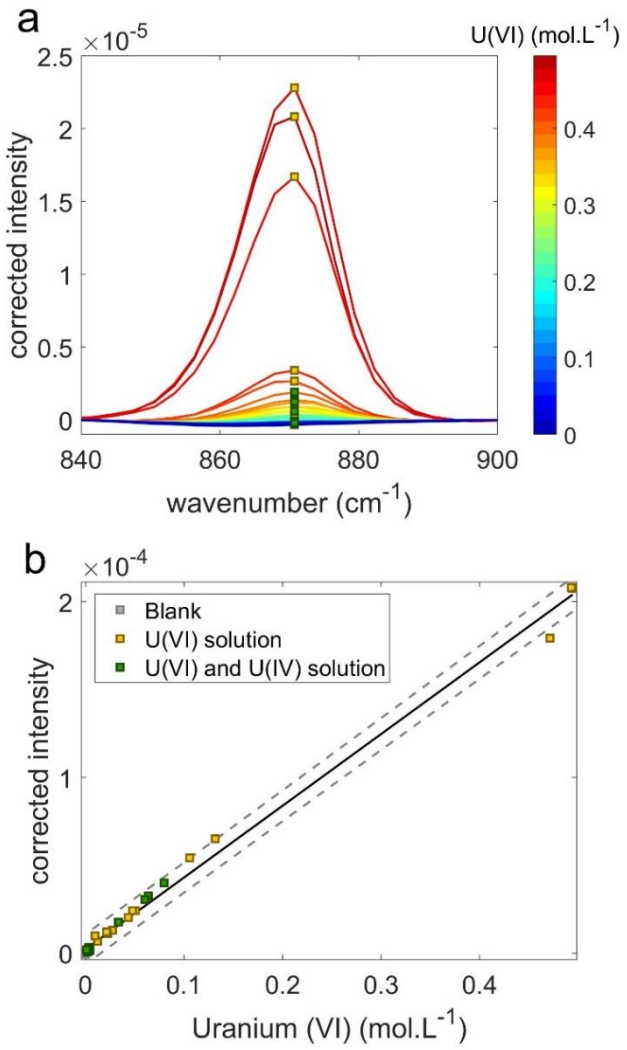

Fig. 6. Raman spectroscopic measurement of uranyl in aqueous solution. a – Raman spectra of aqueous solutions containing uranyl (yellow squares) only and U4+ and uranyl (green squares), preprocessed to reduce background signal. b – Plot of the corrected Raman intensity measurements as a function of uranyl (U(VI)) concentration.

CONCLUSION

The results presented in this paper validate the use of a Photonic Lab on Chip approach for the in-field analysis of actinide solutions. The PhLoCs deployed here allow the

measurement of several types of actinides (Plutonium, Uranium, etc.) in different oxidation states, in constrained nuclear environments such as sealed containers (glove boxes or fume hoods), over wide concentration ranges and above all with the same degree of simplicity and accuracy (i.e. all the measurement capabilities) of a lab-scale UV-Visible spectrometer, but using minute amounts of sample - 140 µL for Pu in a globe box and 10 µL for U solutions under a fume hood, for covering a range of analyzable concentrations of three orders of magnitude - and under hostile conditions. The molar extinction coefficients measured for the different actinides were found to be in good agreement with the values from the literature and the detection limits are well suited for use in on-line process monitoring. Additionally, coupled to a simple but reliable method adapted for processing mixture spectra, they also permitted the quantification of actinide mixtures under different oxidation states when detailed chemometrics are not mandatory.

Finally, the coupling of Raman and UV-Visible spectroscopies at this micro-scale is extremely promising, in particularly in the perspective of the processing of complex mixture spectra including several actinides in different oxidation states.

Moreover, it is obvious that the proposed coupled spectroscopic approach is fully applicable to the characterization of other chemical species such as lanthanides or transition metals, opening up huge perspectives for on-line process monitoring.

AUTHOR INFORMATION

Corresponding Author

* fabrice.lamadie@cea.fr, lamadie@freee.fr

Author Contributions

The manuscript was written through contributions of all authors. All authors have given approval to the final version of the manuscript.

Funding Sources

This work was supported by the Energy Division of CEA (DES-DPE-CYN/PRATA) and partially performed in collaboration with PNNL through the bilateral CEA-US DOE agreement and under research supported by the U.S. Department of Energy, Office of Nuclear Energy, through the Nuclear Technologies R&D Program and by U.S. Department of Energy, Office of Science, through a Small Business Innovation Research (SBIR) grant.

REFERENCES

1. Chiu DT, deMello AJ, Di Carlo D, et al. Small but Perfectly Formed? Successes, Challenges, and Opportunities for Microfluidics in the Chemical and Biological Sciences. *Chem* 2017; 2: 201–223.

2. Wanna NN, Van Hoecke K, Dobney A, et al. Determination of the lanthanides, uranium and plutonium by means of on-line high-pressure ion chromatography coupled with sector field inductively coupled plasma-mass spectrometry to characterize nuclear samples. *J Chromatogr A* 2020; 1617: 460839.

3. Lines AM, Hall GB, Sinkov S, et al. Overcoming Oxidation State-Dependent Spectral Interferences: Online Monitoring of U(VI) Reduction to U(IV) via Raman and UV–vis Spectroscopy. *Ind Eng Chem Res* 2020; 59: 8894–8901.

4. Bürck J. Spectrophotometric determination of uranium and nitric acid by applying partial least-squares regression to uranium(VI) absorption spectra. *Anal Chim Acta* 1991; 254: 159–165.

5. Ganesh S, Khan F, Ahmed MK, et al. Sequential determination of uranium (IV), free acidity and hydrazine in a single aliquot. *J Radioanal Nucl Chem*; 286: 33–37.

6. Meinrath G. Uranium(VI) speciation by spectroscopy. *J Radioanal Nucl Chem* 1997; 224: 119–126.

7. Lines AM, Adami SR, Sinkov SI, et al. Multivariate Analysis for Quantification of Plutonium(IV) in Nitric Acid Based on Absorption Spectra. *Anal Chem* 2017; 89: 9354–9359.

8. Surugaya N, Taguchi S, Sato S, et al. Spectrophotometric Determination of Plutonium in Highly Radioactive Liquid Waste Using an Internal Standardization Technique with Neodymium(III). *Anal Sci* 2008; 24: 377–380.

9. Sinkov SI, Hall GB (ORCID:0000000241937807), Lumetta GJ. Molar Absorptivities of U(VI), U(IV), and Pu(III) in Nitric Acid Solutions of Various Concentrations Relevant to Developing Nuclear Fuel Recycling Flowsheets. *J Radioanal Nucl Chem*; 324. Epub ahead of print 25 May 2020. DOI: 10.1007/s10967-020-07106-8.

10. Bryan SA, Levitskaia TG, Johnsen AM, et al. Spectroscopic monitoring of spent nuclear fuel reprocessing streams: an evaluation of spent fuel solutions *via* Raman, visible, and near-infrared spectroscopy. *Radiochim Acta* 2011; 99: 563–572.

11. Lines AM, Hall GB, Asmussen S, et al. Sensor Fusion: Comprehensive Real-Time, On-Line Monitoring for Process Control via Visible, Near-Infrared, and Raman Spectroscopy. *ACS Sens* 2020; 5: 2467–2475.

12. Mattio E, Lamadie F, Rodriguez-Ruiz I, et al. Photonic Lab-on-a-Chip analytical systems for nuclear applications: optical performance and UV–Vis–IR material characterization after chemical exposure and gamma irradiation. *J Radioanal Nucl Chem* 2020; 323: 965–973.

13. Kim S-Y, Asakura T, Morita Y. Electrochemical and spectroscopic studies of Pu(IV) and Pu(III) in nitric acid solutions. *J Radioanal Nucl Chem* 2013; 295: 937–942.

14. Priyadarshini N, Sampath M, Kumar S, et al. Probing Uranium(IV) Hydrolyzed Colloids and Polymers by Light Scattering. *J Nucl Chem* 2014; 2014: e232967.

15. Bryan SA, Levitskaia TG, Casella AJ, et al. Spectroscopic on-line monitoring for process control and safeguarding of radiochemical streams in nuclear fuel reprocessing facilities. *Adv Sep Tech Nucl Fuel Reprocess Radioact Waste Treat* 2011; 95–119.

16. Clifford AJ, Lackey HE, Nelson GL, et al. Raman Spectroscopy Coupled with Chemometric Analysis for Speciation and Quantitative Analysis of Aqueous Phosphoric Acid Systems. *Anal Chem* 2021; 93: 5890–5896.

17. Lackey HE, Nelson GL, Lines AM, et al. Reimagining pH Measurement: Utilizing Raman Spectroscopy for Enhanced Accuracy in Phosphoric Acid Systems. *Anal Chem* 2020; 92: 5882–5889.

18. Nelson GL, Lackey HE, Bello JM, et al. Enabling Microscale Processing: Combined Raman and Absorbance Spectroscopy for Microfluidic On-Line Monitoring. *Anal Chem* 2021; 93: 1643–1651.

19. Bai X, Li D-M, Chang Z-Y, et al. On-line monitoring of the U(VI) concentration in 30 vol.% TBP/kerosene: an evaluation of real-time analysis in polyetheretherketone (PEEK) containers via Raman spectroscopy. *J Radioanal Nucl Chem* 2015; 305: 643–652.

20. Casella AJ, Levitskaia TG, Peterson JM, et al. Water O-H stretching Raman signature for strong acid monitoring via multivariate analysis. *Anal Chem* 2013; 85: 4120–4128.

21. Daly CA, Streacker LM, Sun Y, et al. Decomposition of the Experimental Raman and Infrared Spectra of Acidic Water into Proton, Special Pair, and Counterion Contributions. *J Phys Chem Lett* 2017; 8: 5246–5252.

22. Rodríguez-Ruiz I, Ackermann TN, Muñoz-Berbel X, et al. Photonic Lab-on-a-Chip: Integration of Optical Spectroscopy in Microfluidic Systems. *Anal Chem* 2016; 88: 6630–6637.

23. Rodríguez-Ruiz I, Lamadie F, Charton S. Uranium(VI) On-Chip Microliter Concentration Measurements in a Highly Extended UV–Visible Absorbance Linearity Range. *Anal Chem* 2018; 90: 2456–2460.

24. Rodríguez-Ruiz I, Teychené S, Van Pham N, et al. Broadcasting photonic lab on a chip concept through a low cost manufacturing approach. *Talanta* 2017; 170: 180–184.

25. Chako NQ. Absorption of Light in Organic Compounds. *J Chem Phys* 1934; 2: 644–653.

26. Juzeliūnas G. Molecule-radiation and molecule-molecule processes in condensed media: a microscopic QED theory. *Chem Phys* 1995; 198: 145–158.

27. Nelson GL, Asmussen SE, Lines AM, et al. Micro-Raman Technology to Interrogate Two-Phase Extraction on a Microfluidic Device. *Anal Chem* 2018; 90: 8345–8353.

28. Nelson GL, Lines AM, Bello JM, et al. Online Monitoring of Solutions Within Microfluidic Chips: Simultaneous Raman and UV–Vis Absorption Spectroscopies. *ACS Sens* 2019; 4: 2288–2295.

29. Long GL, Winefordner JD. Limit of detection. A closer look at the IUPAC definition. *Anal Chem* 1983; 55: 712A-724A.

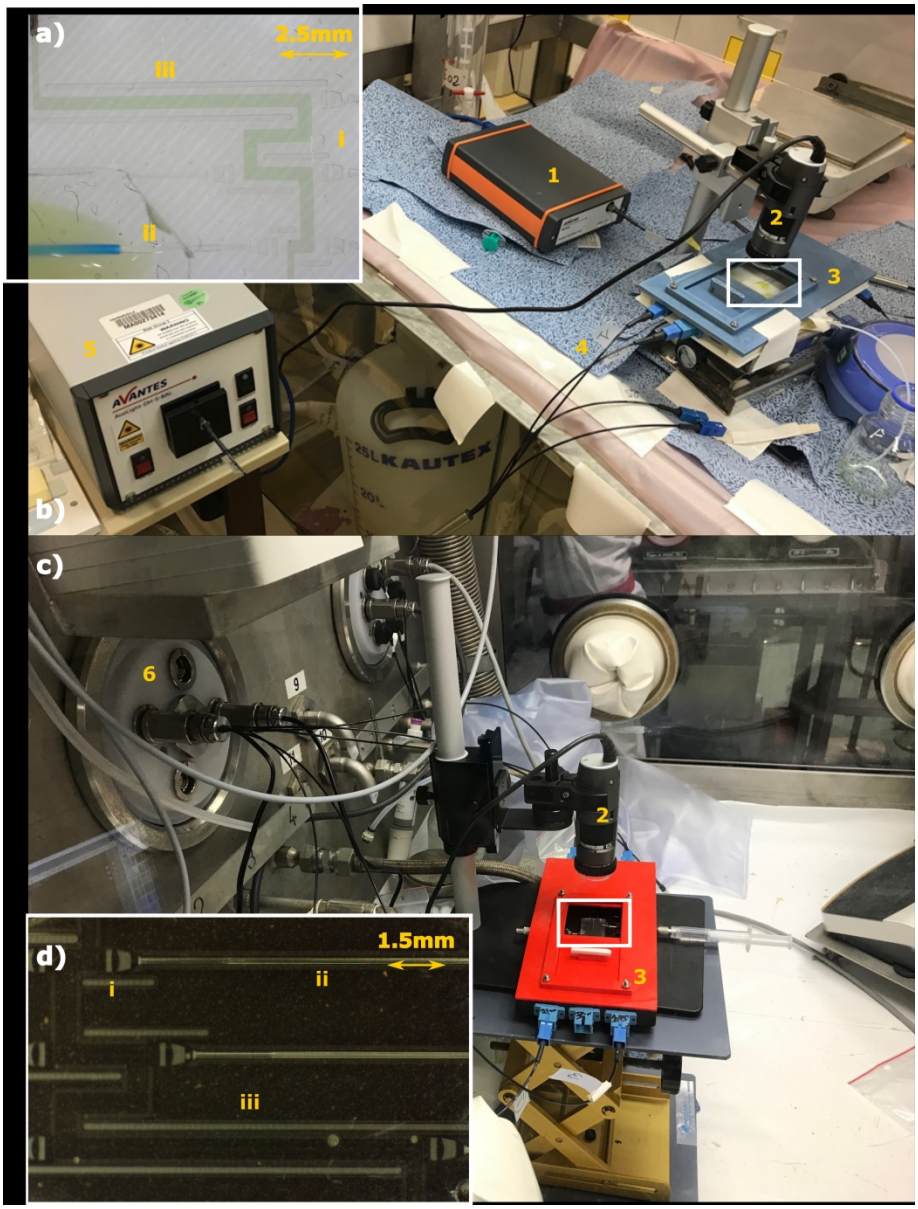

a),d) Zoom of the PDMS chips for uranium (a) and glass chip for plutonium (d), using a handheld microscopic cam-era. The microlenses (i), self-aligning channels for fiber optics positioning (ii), and mirrors (iii), are visible. b), c) Setup implementation in a laboratory fume hood (b) and glove box (c): 1 - Spectrometer, 2 – Handheld microscopic camera, 3 – PhLoc inside its protection holder, 4 - Fibers optics, 5 - Balanced deuterium-halogen light source, 6 - Instrumented hole-plug.

257x337mm (300 x 300 DPI)

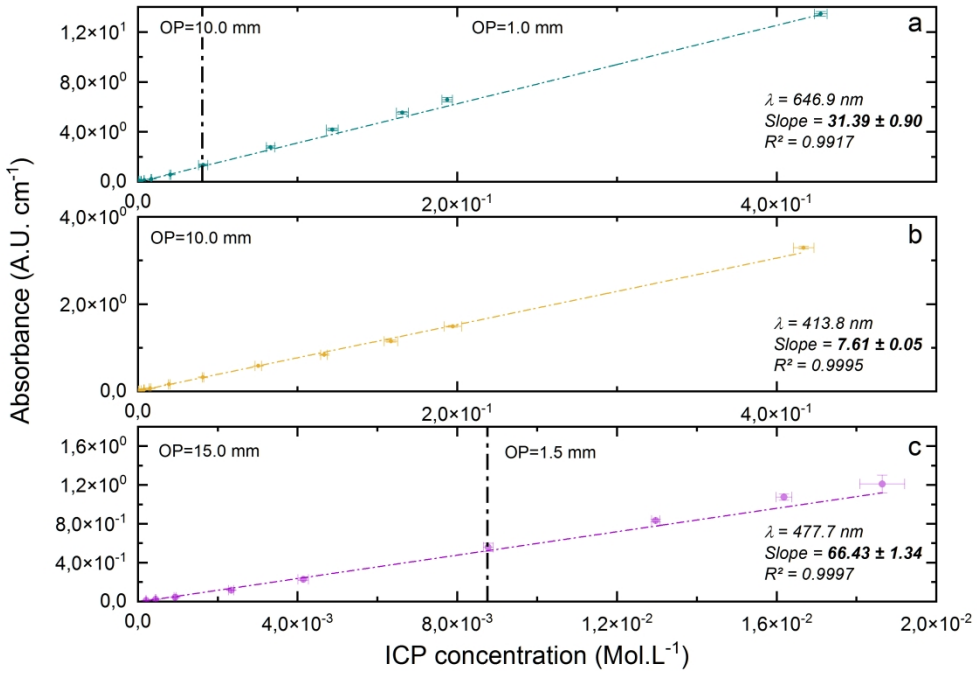

a) Plot of the normalized absorbance measurements (in absorbance units (A.U.) cm^{-1}) as a function of U(IV) concentration. b) Plot of the normalized absorbance measurements (in absorbance units (A.U.) cm^{-1}) as a function of U(VI) concentration. c) Plot of the normalized absorbance measurements (in absorbance units (A.U.) cm^{-1}) as a function of Pu(IV) concentration. Lines represent the least-squares fitting of the experimental data.

289x202mm (300 x 300 DPI)

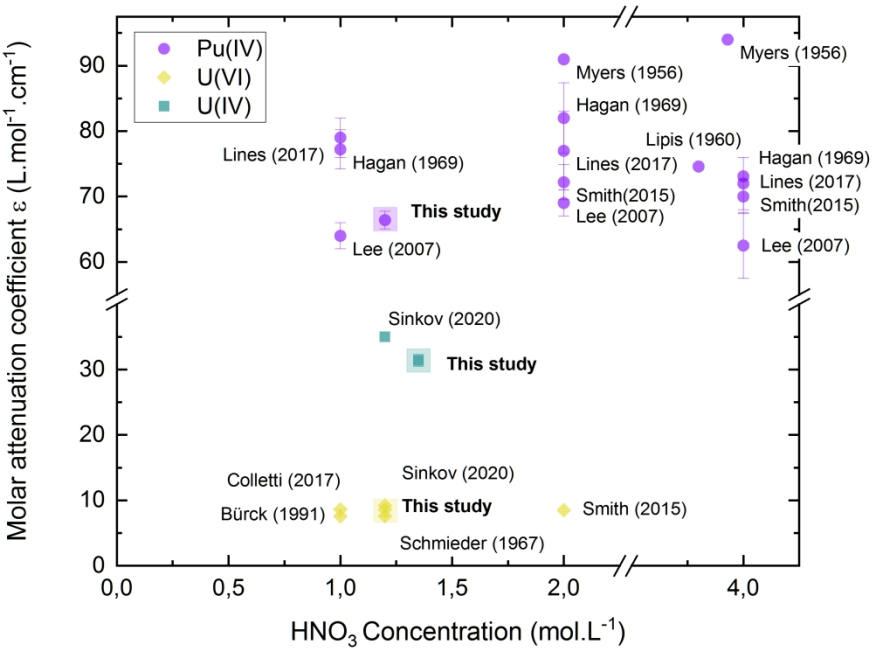

Graphic comparison between the results obtained on opto-fluidic devices and the state of the art from the literature.

272x208mm (300 x 300 DPI)

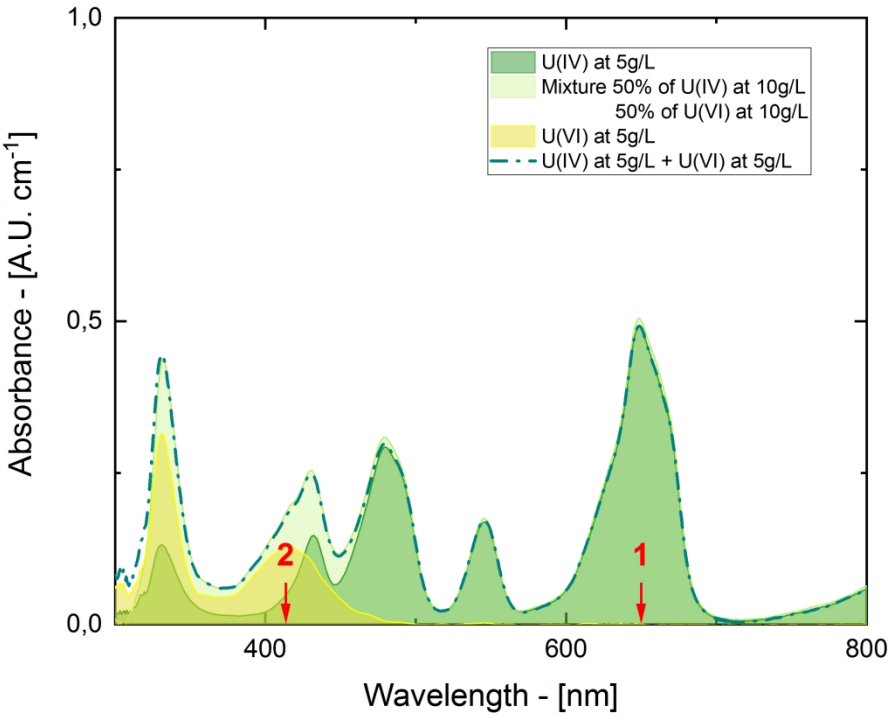

Comparison between the absorbance spectrum of a 50/50 mixture of U(VI) and U(IV) at 10 $g.L^{-1}$ and the absorbance spectra measured on pure U(VI) at 5 $g.L^{-1}$ (yellow) and pure U(IV) at 5 $g.L^{-1}$ (dark green). The dotted green line shows the sum of the absorbance spectra of the two pure com-pounds. The red arrows 1 and 2 denote the wavelengths used for the calculation of the mixtures.

247x196mm (300 x 300 DPI)

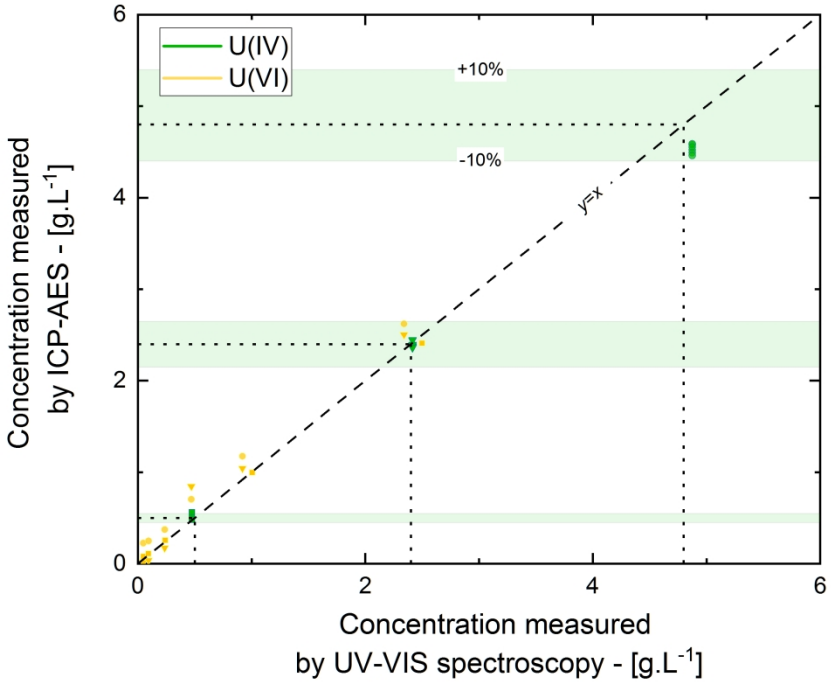

Results obtained on U(IV)/U(VI) mixtures, the yellow sym-bols (triangles, squares, circles) show the results obtained on U(VI), the green symbols show the results obtained on U(IV) - The dotted lines indicate the values measured by ICP-AES. The error bars associated with the measurements have been intentionally excluded to make the figure easier to interpret.

272x208mm (300 x 300 DPI)

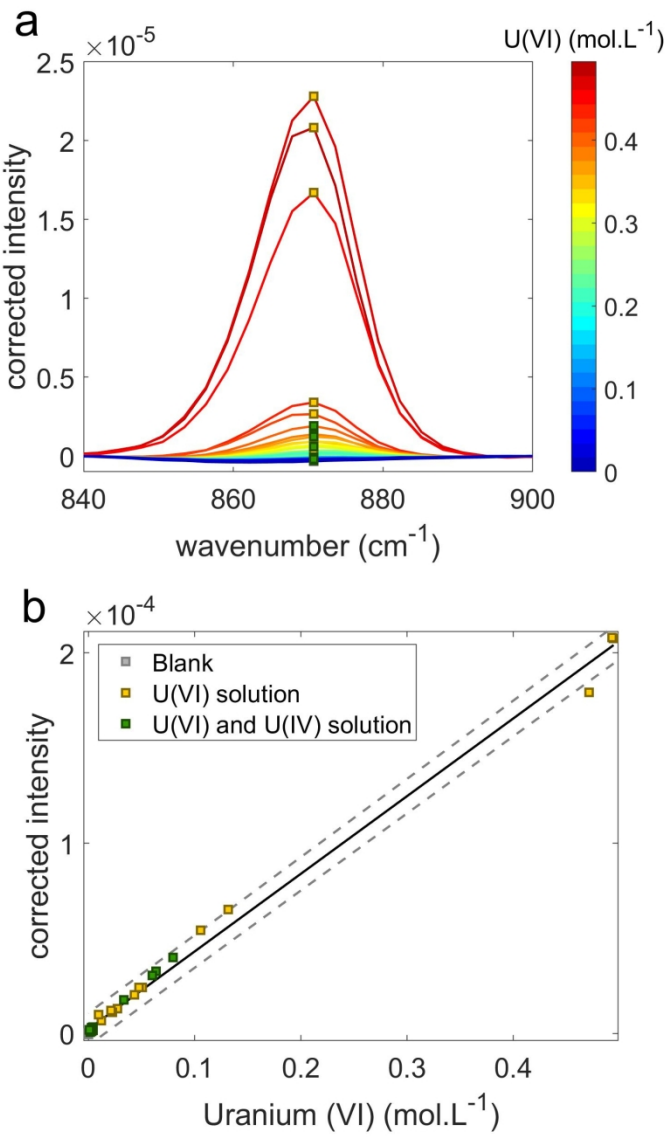

Raman spectroscopic measurement of uranyl in aqueous solution. a – Raman spectra of aqueous solutions containing uranyl (yellow squares) only and U_{4+} and uranyl (green squares), preprocessed to reduce background signal. b – Plot of the corrected Raman intensity measurements as a function of uranyl (U(VI)) concentration.

529x918mm (72 x 72 DPI)

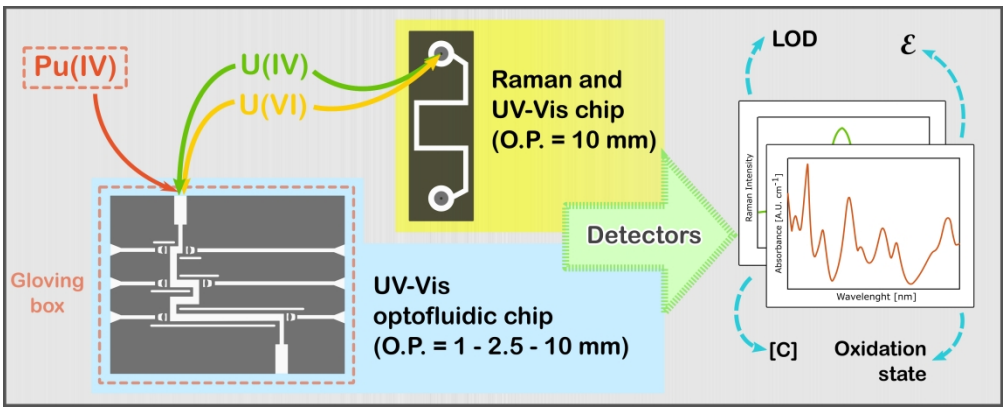

893x357mm (118 x 118 DPI)